Strength reduction factors for wind and earthquake effects

Martinez-Vazquez, Pedro

DOI:
10.1680/jstbu.16.00086

Document Version
Peer reviewed version

Citation for published version (Harvard):
Martinez-Vazquez, P 2017, 'Strength reduction factors for wind and earthquake effects', *Institution of Civil Engineers. Proceedings. Structures and Buildings*. https://doi.org/10.1680/jstbu.16.00086

Structures and Buildings

Strength Reduction Factors for Wind and Earthquake Effects

--Manuscript Draft--

Manuscript Number:	SB-D-16-00086R2
Full Title:	Strength Reduction Factors for Wind and Earthquake Effects
Article Type:	General paper
Corresponding Author:	Pedro Martinez-Vazquez The University of Birmingham Birmingham, UNITED KINGDOM
Corresponding Author Secondary Information:	
Corresponding Author's Institution:	The University of Birmingham
Corresponding Author's Secondary Institution:	
First Author:	Pedro Martinez-Vazquez
First Author Secondary Information:	
Order of Authors:	Pedro Martinez-Vazquez
Order of Authors Secondary Information:	
Abstract:	Strength reduction factors are typically estimated for seismic events ignoring the influence of wind. However, if we consider that strong earthquakes are commonly followed by a number of moderate to strong aftershocks and that wind is constantly flowing, often with low to medium intensity but occasionally reaching high speeds, then the assumption of using earthquake ground records only to determine strength reduction factors seems questionable. In this paper is shown that the combined action of strong winds and earthquakes, however its low probability of occurrence, would considerably increase the ductility demand of buildings and cause a decrease of strength reduction factors calculated by ignoring wind. The paper examines the non-linear performance of single degree of freedom systems subject to various levels of winds and earthquake load and deals with the estimation of strength reduction factors associated to those multi-hazard scenarios.

Article type: Research
Date text written or revised: March 2017
Number of words in main text: 6221 [including Tables]
Number of figures: 10

Strength Reduction Factors for Wind and Earthquake Effects

P Martinez-Vazquez, PhD

School of Engineering, University of Birmingham, B15 2TT, United Kingdom

Tel.: +44(0) 121 414 5059; Email: p.vazquez@bham.ac.uk

Abstract

Strength reduction factors are typically estimated for seismic events ignoring the influence of wind. However, if we consider that strong earthquakes are commonly followed by a number of moderate to strong aftershocks and that wind is constantly flowing, often with low to medium intensity but occasionally reaching high speeds, then the assumption of using earthquake ground records only to determine strength reduction factors seems questionable. In this paper is shown that the combined action of strong winds and earthquakes, however its low probability of occurrence, would considerably increase the ductility demand of buildings and cause a decrease of strength reduction factors calculated by ignoring wind. The paper examines the non-linear performance of single degree of freedom systems subject to various levels of winds and earthquake load and deals with the estimation of strength reduction factors associated to those multi-hazard scenarios.

Key words: design methods & aids; seismic engineering; wind load & aerodynamics

List of symbols

A	: Area exposed to wind	u	: Displacement
c	: Weibull scale parameter	$\bar{U}$	: Average wind velocity
C_D	: Drag coefficient	W	: Building width
F	: Force	z	: Vertical coordinate
H	: Building height	z_0	: Roughness length
I	: Turbulence intensity		
L	: Building length	μ	: Inelastic level
m	: Mass	φ	: Modal shape
n_0	: Fundamental frequency	Γ	: Mass to volume ratio
k	: Weibull shape parameter	σ	: Root mean square
K	: Stiffness	ρ	: Density of air
R	: Strength reduction factor	ω	: Frequency
T	: Period of vibration	ξ	: Fraction of critical damping

1. Introduction

The use of strength reduction factors (SRFs) is adopted by major codes around the world for performance-based design, such is the case of NBC (2015), EC8 (2011), FEMA P695 (2009), and ANSI/ASCE 7-95 (1996), to mention some. Elastic response spectra and SRFs can thus be used to determine design forces that are lower than those limiting structural response to the linear-elastic range; hence accepting that certain level of structural damage may occur which would trigger minor, moderate or major actions for repair. A number of approaches to calculate SRFs there exist. Newmark and Hall (1982) provided a comprehensive study on the relationship between earthquake spectra and design practices involving various levels of conservatism and hazard. In Miranda and Bertero (1994) a number of earlier approaches to compute SRFs are critically compared. That include models by Newmark and Hall (1973), Riddell and Newmark (1979), Lai and Biggs (1980), Elghadamsi and Moraz (1987), Ridell, Hidalgo, and Cruz (1989), Hidalgo and Arias (1990), Nassar and Krawinkler (1991), and Vidic, Fajafar, and Fischinger (1992). Miranda and Bertero (1994) showed that SRFs are influenced by the ductility demand, structural period, and soil conditions. The latter also reviewed in Miranda (1993) where it was concluded that soil type considerations strongly influence design forces. In Gillie et al. (2010) and Chopra and Chintanapakdee (2001) it was pointed out that although epicentral distance(ED) can have an impact on the magnitude of SRFs, models to estimate SRFs, formulated without distinction of ED, can be used for near-fault (NF) areas if appropriate consideration of spectral regions is made. All these studies assume however that earthquake and wind events are uncorrelated. This assumption seems reasonable when accepting that the structure's lifetime assumed for either design condition does limit their joint probability of occurrence. However little to no research has been produced for cases in which major earthquake events clash with low to moderate winds whose probability of occurrence is significant or when, however it is low probability of occurrence, major seismic and wind events occur simultaneously. The latter does not seem unlikely after all if we consider the number of aftershocks that usually follow major earthquake events. For example the earthquake that hit Nepal in 2015 (Ms =7.8) killing more than 8,000 (Amos, 2015) was followed by 30 aftershocks of Ms < 5 occurring within three weeks and killing 200 more. The earthquake that hit the Sichuan Province in China in 2008 (Ms =7.9) killing over 87,000 (Daniell et al., 2011) was followed by 12 weeks with 42 aftershocks ranging in magnitude between 5 < Ms < 6.4. If we add this to the fact that wind is constantly flowing with a minimum speed that is equal to the average local wind velocity, then the current design assumptions concerning the unrelated action of wind and earthquakes do not seem conservative. The present paper thus deals with the estimation of SRFs covering the combined effect of earthquakes occurring simultaneously with wind flowing at mean speeds ranging between 0.5 ms^{-1} and 20 ms^{-1}. The earthquake database used in the study includes near-fault (NF) and far-fault (FF) events which enable to establish a comparison of results with existing approaches to determine SRFs (formulated by using a similar criteria) although the influence of ED on SRFs is also examined.

2. Strength reduction factors: an overview

The basic idea for estimating SRFs is the balance between potential and strain energy acting on a structure which induces its maximum displaced configuration. This deformation process would include two stages namely linear elastic and plastic. Fig. 1 illustrates the transition from elastic to plastic behaviour of one *sdof* oscillator. In this figure u represents displacement, F is the restoring force required to keep inelastic displacements within the limit of the ductility factor μ.

FIGURE 1

The definition of SRF as in Miranda (1993) is given by Eq. (1). That is the ratio between the force required to keep the structural performance elastic and the force that is induces inelastic displacements associated to a certain ductility μ. The ductility factor is defined by Eq. (2).

$$R_\mu = \frac{F_y(\mu=1)}{F_y(\mu=\mu)} \quad (1)$$

$$\mu = \frac{u_{max-inelastic}}{u_y} \quad (2)$$

$$\ddot{u}(t) + 2\xi\omega\dot{u}(t) + \frac{F(u)}{m} = -\ddot{y}(t) \quad (3)$$

The equation of motion of a single-degree of freedom (*sdof*) oscillator is given by Eq. (3), where ξ represents the fraction of critical damping, ω is the undamped frequency of vibration, m is the mass, and $\ddot{y}(t)$ is the base acceleration. Eq. (1-3) are thus related when solving the equation of dynamic equilibrium in order to find the restoring force *F(u)* to avoid the target value of μ being exceeded. This method has been widely used to determine inelastic response spectra considering at least three non-linear load-deformation models: elastoplastic, bilinear, and stiffness degrading – see for example Miranda and Bertero (1994), Chopra and Goel (1999), and Riddell et al. (2002). In the present research the elastoplastic model is adopted when running the non-linear analysis of *sdof* systems.

3. Earthquake record database

In this study 40 earthquake ground motions covering magnitudes 5 < Ms < 8 and recorded on alluvium sites were considered. These were downloaded from the PEER Ground Motion Database (Pacific Earthquake Research Centre, 2016) considering all types of fault, ED of up to 57 km and damping ratio of 5% - see Table 1. In Miranda (1993) it is observed that the factors that influence the intensity, frequency content and duration of ground motions are the earthquake magnitude, distance to the source, and soil type; whereas SRFs calculated on alluvium sites tend to be lower than those recorded on rock, for systems with periods between 1.3 and 2.4 s although the opposite happens for periods below 1.3 s. The differences in terms of lateral strength of structures on these soil types however are slightly different as the curves that define the relationship R_μ-T for firm and alluvium sites show similar patterns. In contrast, SRFs calculated on soft soils show large differences with respect to those calculated on rock or alluvium and therefore using those to design structures without distinction of the soil type can considerably under- or over-estimate ductility demands (Miranda, 1993). On the other hand, Gillie et al. (2010), Bray and Rodriguez-Marek (2004), and Chopra and Chintanapakdee (2001), suggest that NF earthquakes (e.g. ED < 20 km) could have more devastating effects on structures that FF ones due to energy contents stored in relatively long-term pulses embedded in the ground motion. Taking into account that the aim of this investigation is to examine the variation of SRFs associated to multi-hazard scenarios, the earthquake database used for the present study includes events recorded on alluvium only whilst in principle makes no distinction of ED. This limits the scope of this study to alluvium soils and, without much variation, to firm soils. The potential impact of ED on the SRFs estimated herein is discussed in section 6.

Table 1. Earthquake record database used in the present study

#	Earthquake	Magnitude	Epicentral Distance Km	vs_{30} ms^{-1}	PGA g
1	Helena Montana-01, 10/31/1935, Carroll College, 180	6	2.86	593.35	0.16
2	Helena Montana-01, 10/31/1935, Carroll College, 270	6	2.92	551.82	0.16
3	Northwest Calif-01, 9/12/1938, Ferndale City Hall, 45	5.5	53.58	219.31	0.15
4	Northwest Calif-03, 10/8/1951, Ferndale City Hall, 224	5.8	53.77	219.31	0.11

5	Izmir Turkey, 12/16/1977, Izmir, L	5.3	3.21	535.24	0.42
6	Izmir Turkey, 12/16/1977, Izmir, T	5.3			0.13
7	Dursunbey Turkey, 7/18/1979, Dursunbey, L	5.34	9.15	585.04	0.18
8	Dursunbey Turkey, 7/18/1979, Dursunbey, T	5.34			0.24
9	Imperial Valley-02, 5/19/1940, El Centro Array #9, 180	6.95	6.09	213.44	0.25
10	Imperial Valley-02, 5/19/1940, El Centro Array #9, 270	6.95			0.15
11	Northern Calif-01, 10/3/1941, Ferndale City Hall, 225	6.4	44.68	219.31	0.10
12	Northern Calif-01, 10/3/1941, Ferndale City Hall, 315	6.4			0.12
13	Northern Calif-03, 12/21/1954, Ferndale City Hall, 44	6.5	27.02	219.31	0.16
14	Northern Calif-03, 12/21/1954, Ferndale City Hall, 314	6.5			0.16
15	Borrego Mtn, 4/9/1968, El Centro Array #9, 180	6.63	45.66	213.44	0.13
16	San Fernando, 2/9/1971, Castaic - Old Ridge Route, 21	6.61	22.63	450.28	0.32
17	San Fernando, 2/9/1971, Castaic - Old Ridge Route, 291	6.61			0.28
18	San Fernando, 2/9/1971, LA - Hollywood Stor FF, 90	6.61	22.77	316.46	0.22
19	San Fernando, 2/9/1971, LA - Hollywood Stor FF, 180	6.61			0.16
20	San Fernando, 2/9/1971, Lake Hughes #1, 21	6.61	27.4	425.34	0.15
21	San Fernando, 2/9/1971, Lake Hughes #12, 21	6.61	19.3	602.1	0.38
22	San Fernando, 2/9/1971, Lake Hughes #12, 291	6.61			0.28
23	Imperial Valley-06, 10/15/1979, Bonds Corner, 140	6.53	2.66	223.03	0.52
24	Imperial Valley-06, 10/15/1979, Bonds Corner, 230	6.53			0.77
25	Imperial Valley-06, 10/15/1979, El Centro Array #4, 140	6.53	7.05	208.91	0.48
26	Imperial Valley-06, 10/15/1979, El Centro Array #4, 230	6.53			0.27
27	Imperial Valley-06, 10/15/1979, El Centro Array #5, 140	6.53	3.95	205.63	0.33
28	Imperial Valley-06, 10/15/1979, El Centro Array #5, 230	6.53			0.38
29	Imperial Valley-06, 10/15/1979, El Centro Array #7, 140	6.53	0.56	210.51	0.34
30	Imperial Valley-06, 10/15/1979, El Centro Array #7, 230	6.53			0.47
31	Kern County, 7/21/1952, Taft Lincoln School, 21	7.36	38.89	385.43	0.14
32	Kern County, 7/21/1952, Taft Lincoln School, 111	7.36			0.15
33	Taiwan SMART1(45), 11/14/1986, SMART1 C00, EW	7.3	56.01	309.41	0.12
34	Taiwan SMART1(45), 11/14/1986, SMART1 C00, NS	7.3			0.15
35	Taiwan SMART1(45), 11/14/1986, SMART1 O02, EW	7.3	57.13	285.09	0.16
36	Taiwan SMART1(45), 11/14/1986, SMART1 O02, NS	7.3			0.24
37	Cape Mendocino, 4/25/1992, Petrolia, 0	7.01	8.18	422.17	0.58
38	Cape Mendocino, 4/25/1992, Petrolia, 90	7.01			0.66
39	Landers, 6/28/1992, Lucerne, 260	7.28	2.19	1369	0.65
40	Landers, 6/28/1992, Lucerne, 345	7.28			0.61

4. Strength reduction factors for zero-wind load

In order to validate the inelastic response model used here the earthquake records listed in Table 1 were applied to a number of single oscillators characterised by their vibration period *(T)*, level of inelastic deformation *(μ)*, and with 5% damping. Eq. (3) was solved through iterations for each value of *T* and μ. The value of the restoring force $F(u)$ was varied until the ratio $u_{umax-inelastic} / u_y$ - where u_y is the yielding deformation, matched the target value of μ. The corresponding SRF, R_μ, was then estimated by using Eq. (1). In Fig. 2-4 the estimated SRFs are compared with the reference models suggested by Ridell, Hidalgo, and Cruz (1989), Hidalgo and Arias (1990), Nassar and Krawinkler (1991), Vidic, Fajafar and Fischinger (1992), and Miranda and Bertero (1994).

FIGURES 2 TO 4

Fig. 2-4 show that the estimated SRFs capture the main features of the reference models. The curves show a rapid increase in the interval $0 \leq T \leq 1$ followed by a change of direction into a region which tends to be flat until ~ T = 3 s. The estimated values of R_μ tend to increase afterwards as suggested by Hidalgo and

Arias (1990) although not at the same rate. The major differences are thus in the region $3 \leq T \leq 5$ for high ductility levels. Table 2 shows that the estimated curves differ on average in ~ $\pm$ 8% from reference models whilst Fig. 5 shows a comparison between estimated and reference values of R_μ / μ, averaged across μ values.

Table 2. Estimated under- and over-estimation of R_μ with respect to reference models

Reference Model	Under-E (%)	Over-E (%)
Ridell, Hidalgo and Cruz, 1989	5.22	7.69
Hidalgo and Arias, 1990	10.67	7.59
Nassar and Krawinkler, 1991	8.34	8.63
Vidic, Fajafar and Fischinger, 1992	4.53	9.06
Miranda and Bertero, 1994	11.4	8.19

FIGURE 5

Fig. 5 shows that the variation of $\overline{R_\mu/\mu}$ falls within the limits established by the reference models and therefore the inelastic response model implemented for this research was considered adequate.

5. Wind and earthquake loading

Eq. (3) can be used to calculate the inelastic response of *sdof* systems subject to earthquake and wind. For point-like structures the input load can simply be obtained by superimposing both actions thus assuming these act simultaneously whilst randomly off-phase. This would enable to obtain the total acting force by using Eq. (4) – where ρ represents the density of air, C_D is a drag coefficient, $\overline{U}$ and $u(t)$ are the mean and dynamic wind velocity components, and A is the area exposed to wind. An equivalent load scheme can be established for multiple-degree of freedom *(mdof)* systems through the generalisation of loads as in Eq. (5), where F^*_{EQ} and F^*_W represent generalised earthquake and wind load respectively.

$$F_T(t) = m\ddot{y}(t) + \frac{1}{2}\rho C_D[\overline{U} + u(t)]^2 A \quad (4)$$

$$F_T(t) = F^*_{EQ}(t) + F^*_W(t) \quad (5)$$

There is a fundamental difference between wind and earthquake load acting on large areas. The horizontal accelerations induced by earthquakes along the height of structures are assumed to be fully correlated (Chopra, 1995) whereas the corresponding wind forces are not (Dyrbye and Hansen, 1997). The correlation of wind forces depends on the spatial distribution of wind gusts and that is usually taken into account through suitable correlation laws such as those proposed by Vickery (1970) and Tanaka and Lawen (1986) together with admittance functions such as that proposed by Davenport (1967). This implies that the ratio F^*_{EQ}/F^*_W will vary from building to building. Besides, no direct relationship can be established between the mass which relates to earthquake load and the effective area exposed to wind. In this context, is required to ensure that the value of $F_T(t)$ used to solve Eq. (3) is representative of full-scale structures. For this reason the mean ratio F^*_{EQ}/F^*_W is calculated for three buildings as discussed below.

5.1 Analysis of full-scale structures

The analysis of the buildings consisted on generalising their mechanical properties as well as earthquake and wind forces. Generalised forces *(F*)* and mass *(M*)* were calculated through Eq. (6) where Υ *(z)*

represents force or structural mass per unit length, z is a vertical coordinate, and ϕ is the fundamental modal shape which was approximated by $\phi(z)=(z/H)^{\beta}$ – with β = 1.5 and taking H as the height of the building. The generalised stiffness was obtained with $K^* = 4\pi^2 n_0^2 M^*$, where n_0 is the fundamental frequency of the system.

$$\Upsilon^* = \int_0^H \phi(z)^2 \Upsilon(z)\, dz \quad (6)$$

The estimation of $F_W^*(t)$ requires knowledge of the wind field which fluctuates along the height $0 \leq z \leq H$. To that end the computer simulation reported in Martinez-Vazquez and Rodriguez-Cuevas (2007) - which is based on the algorithm proposed by Vanmarcke et al. (1993), was revisited. The statistics of the simulated time series and cross-correlation results are provided in Tables 3-4 for the case in which $\bar{U}_t$ = 20 ms^{-1}. The turbulence intensity, which is defined as $I = \sigma_u / \bar{U}_t$ – where σ_u is the root mean square *(rms)* of the fluctuating wind speed, is taken as 0.295 (measured at 10 m above the ground) whilst the roughness length *(z_0)* equals 0.3 m. The reader is referred to Martinez-Vazquez and Rodriguez-Cuevas (2007) for further details on the computer simulation.

Table 3. Calculated statistics of simulated wind time series

Stats \ z (m)	10	40	75	100	140	170	200
$\bar{U}_t$	20.00	30.21	36.21	39.79	42.95	45.39	47.77
$\bar{U}_s$	19.86	29.88	35.14	38.62	41.69	44.05	46.32
$I_{u,t}$	0.295	0.270	0.244	0.221	0.195	0.172	0.146
$I_{u,s}$	0.295	0.206	0.173	0.153	0.135	0.122	0.108

Table 4. Cross correlation results

Point	1	2	3	4	5	6	7
1	**1.0000**	0.4737	0.4100	0.2255	0.2134	-0.0052	-0.0591
2	0.4237	**1.0000**	0.6224	0.3814	0.2928	0.1594	0.0892
3	0.2090	0.4767	**1.0000**	0.6510	0.5322	0.2694	0.2860
4	0.1176	0.2605	0.5419	**1.0000**	0.7333	0.4118	0.4189
5	0.0653	0.1408	0.2895	0.5322	**1.0000**	0.6122	0.5377
6	0.0394	0.0831	0.1690	0.3092	0.5798	**1.0000**	0.5934
7	0.0231	0.0479	0.0961	0.1748	0.3265	0.5625	**1.0000**

Table 3 shows that the average ratio $\bar{U}_t$ / $\bar{U}_s$ is equal to 1.028 whereas the mean square error associated to the simulated turbulence intensity is 0.002. Table 4 shows the target and calculated cross-correlation in the lower and upper triangular matrices respectively whilst Point 1 corresponds to that located at z = 10 m. The overall mean square error across cross-correlation results is 0.0073 which was considered acceptable for the purpose of this research.

The main characteristics of the prototype building are shown in Fig. 6. Three full-scale structures covering heights of 20 m, 100 m, and 180 m were targeted. These have structural mass of 160 kgm^{-3} and are assumed to dynamically respond in their fundamental mode. It is acknowledged that higher-order modes can have meaningful contribution to the total response of flexible structures – for example those with T > 2s, however the fact that modal participation factors are unrelated to the type of excitation suggest that the approximation based on the fundamental mode does not lead to unrealistic results, since the load-response estimation of earthquake and wind load would vary at similar rates when accounting for higher-

order modes. The geometry and generalized properties of the target buildings are presented in Table 5 together with the ratio F_{EQ}^*/F_W^* representing the average proportion of earthquake and wind forces estimated over a period of 3 min.

FIGURE 6

Table 5. Characteristics of target buildings and estimated values of F_{EQ}^*/F_W^*

Building 1	H = 180 m; L = 30 m; W = 45 m; n_0 = 0.239 Hz; M*= 1.14x10^7 kg									
	Dir-X					Dir-Y				
$\bar{U}$ (ms^{-1})	0.5	5	10	15	20	0.5	5	10	15	20
F_{EQ}^*/F_W^*	474.79	4.75	1.19	0.53	0.3	906.42	9.06	2.27	1.01	0.56
Building 2	H = 100 m; L = 16.67 m; W = 25 m; n_0 = 0.372 Hz; M*= 1.86x10^6 kg									
	Dir-X					Dir-Y				
$\bar{U}$ (ms^{-1})	0.5	5	10	15	20	0.5	5	10	15	20
F_{EQ}^*/F_W^*	183.3	1.83	0.46	0.2	0.11	349.93	3.5	0.87	0.39	0.22
Building 3	H = 20 m; L = 6 m; W = 8 m; n_0 = 1243 Hz; M*= 4.28x10^4 kg									
	Dir-X					Dir-Y				
$\bar{U}$ (ms^{-1})	0.5	5	10	15	20	0.5	5	10	15	20
F_{EQ}^*/F_W^*	78.68	0.79	0.2	0.09	0.05	128.32	1.28	0.32	0.14	0.08

The results shown in Table 5 reflect the predicted variability of earthquake and wind forces. As the area exposed to wind reduces wind gusts increase correlation which results in a lower value of F_{EQ}^*/F_W^* whereas the value of this parameter decreases with $\bar{U}$ as *M** keeps constant. Noting that, however the PGA of the seismic actions considered in this study ranges between 0.1g and 0.77g, the variability of the ratio F_{EQ}^*/F_W^* amongst different ranges of PGA e.g. 0.1-0.3PGA, 0.3-0.5PGA, and 0.5-0.7PGA is within reasonable limits. The results in Table 1 are summarised in Table 6 after averaging the values of F_{EQ}^*/F_W^* considering all earthquake records and wind directions. In addition, each building is characterised through the parameter $\Gamma = \frac{M^*}{\sqrt{H^2+W^2+L^2}}$ - which expressed in Ton·m^{-1} turns out to be of 60.43, 17.78, and 1.91, for Buildings 1, 2 and 3, respectively.

Table 6. Variation of F_{EQ}^*/F_W^* with Γ and Ū

Γ (Ton·m^{-1})	$\bar{U}$ (ms^{-1})				
	0.5	5	10	15	20
60.43	690.61	6.91	1.73	0.77	0.43
17.78	266.61	2.67	0.67	0.30	0.17
1.91	103.5	1.03	0.26	0.11	0.06

The following section presents SRFs estimated for each value of Γ and $\bar{U}$ shown in Table 6. Note that the full-scale analysis undertaken above span a wide range of building geometries and load configurations but bearing in mind the assumptions made to synthesise the ratio F_{EQ}^*/F_W^* within 15 such combinations.

6. Strength reduction factors for multi-hazard scenarios

In line with the previous sections the inelastic response of a group of *sdof* systems subject to earthquake and wind was calculated. Earthquake load was generated by using the database presented in Table 1 whilst wind loading for the point-like systems was simulated by using the algorithm described in the Appendix - hence no wind data recorded during the actual earthquake events was required. For this analysis the ratio F_{EQ}^{*}/F_{W}^{*} specified in Table 6 was observed for estimating $F_T(t)$. The total load was obtained with Eq. (9) whilst the inelastic response of the oscillators was calculated with Eq. (3). Fig. 7-11 shows the results of these analyses where SRFs for multi-hazard scenarios are represented as R'_{μ}.

FIGURES 7 TO 11

Fig. 7-11 shows that SRFs vary with Γ and $\overline{U}$. The impact of $\overline{U}$ in the value of R'_{μ} is remarkable. The average decrease of is of 19.5%, 37.3%, and 42% for when Γ is of 60.43, 17.78, and 1.91 respectively, but it can be up to 53%, 62.9%, and 67.8%, respectively, for when μ = 6 and $\overline{U}$= 20 ms^{-1}. There is also a decrease associated with μ and T which can be better appreciated when plotting R'_{μ} / R_{μ} as in Fig. 12-13, where R_{μ} represents SRFs relative to the zero-wind load condition.

FIGURES 12 TO 13

Fig. 12-13 shows that the decrease of R'_{μ} / R_{μ} is considerable even for low values of $\overline{U}$. The average reduction of SRFs when $\overline{U} = 5$ ms^{-1} is of 0.008%, 13.5%, 24.7%, 33%, 39%, and 43.5% associated to μ = 1, 2, 3, 4, 5, and 6 respectively. SRFs also decrease at higher rates when T increases although the variation of R'_{μ} / R_{μ} tends to slow down as $\overline{U}$, μ and T increase. The highest changes occur within the intervals 0.5 $\leq$ $\overline{U}$ $\leq$ 10, 0 $\leq$ T $\leq$ 1, and 1 $\leq$ μ $\leq$ 3.

The influence of Γ in the value of SRFs has also been identified. The decrease of the ratio R'_{μ} / R_{μ} can be of up to ~40% on average (with respect to μ) for example when 5 ms^{-1} $\leq$ $\overline{U}$ whilst the largest impact seem to occur in the neighbourhood of T = 1 s. The estimated decrease of R'_{μ} / R_{μ} averaged across all ductility levels is of 7.6% and 28.5% when $\overline{U} = 0.5$ ms^{-1} and $\overline{U} = 5$ ms^{-1} respectively. Fig. 14 provides an overview of the influence of Γ on the ratio R'_{μ} / R_{μ}.

FIGURE 14

The results shown in Fig. 14 reflect the variation of F_{EQ}^{*}/F_{W}^{*} implicit in Table 6. This is that F_{EQ}^{*}/F_{W}^{*} decreases with Γ and therefore the influence of wind load on the inelastic response of structures increases with respect to that due to the sole action of earthquake load. The fact that R'_{μ} / R_{μ} decreases at higher rates with low values of Γ suggests that relatively small structures, where wind gusts are better correlated, are more susceptible to exceed the target ductility levels than relatively large structures if these were designed with SRFs calculated under the zero-wind condition. However relatively large structures i.e. those associated with large values of Γ, are not exempt of such an underestimation of inelastic ductility. The results discussed above are summarised in Tables 7-8 where the variation of R'_{μ} / R_{μ} with $\overline{U}$, Γ and μ is provided. These results correspond to the ratio R'_{μ} / R_{μ} averaged over values of T $\leq$ 2 s (Table 7) and T > 2 s (Table 8). The distinction over T is to illustrate variations of R'_{μ} / R_{μ} for rigid and flexible buildings.

Table 7. Variation of R'_μ / R_μ with $\overline{U}$, Γ and μ, averaged across T ≤ 2 s.

Γ = 60.43	μ					
$\overline{U}$ (ms^{-1})	1	2	3	4	5	6
0.5	1.022	0.985	0.976	0.946	0.918	0.910
5	1.009	0.955	0.938	0.906	0.894	0.881
10	0.998	0.932	0.897	0.843	0.818	0.781
15	0.997	0.901	0.829	0.756	0.718	0.675
20	1.008	0.885	0.793	0.725	0.691	0.646
Γ = 17.78	μ					
$\overline{U}$ (ms^{-1})	1	2	3	4	5	6
0.5	1.019	0.996	0.975	0.953	0.926	0.930
5	1.005	0.946	0.921	0.876	0.852	0.815
10	1.006	0.866	0.771	0.695	0.655	0.618
15	1.004	0.849	0.754	0.677	0.641	0.602
20	1.025	0.827	0.735	0.645	0.590	0.537
Γ = 1.91	μ					
$\overline{U}$ (ms^{-1})	1	2	3	4	5	6
0.5	1.020	1.006	1.005	1.001	1.001	0.996
5	1.005	0.920	0.853	0.788	0.753	0.715
10	1.006	0.821	0.715	0.642	0.599	0.561
15	1.007	0.744	0.615	0.536	0.490	0.455
20	1.007	0.719	0.585	0.507	0.462	0.425

Table 8. Variation of R'_μ / R_μ with $\overline{U}$, Γ and μ, averaged across T > 2 s.

Γ = 60.43	μ					
$\overline{U}$ (ms^{-1})	1	2	3	4	5	6
0.5	0.999	1.003	0.997	0.983	0.961	0.975
5	0.998	0.959	0.865	0.793	0.734	0.692
10	0.987	0.889	0.762	0.676	0.608	0.557
15	0.996	0.762	0.599	0.499	0.426	0.376
20	0.996	0.753	0.588	0.481	0.405	0.353
Γ = 17.78	μ					
$\overline{U}$ (ms^{-1})	1	2	3	4	5	6
0.5	0.998	1.000	0.982	0.973	0.945	0.953
5	0.995	0.936	0.832	0.749	0.677	0.628
10	0.995	0.768	0.613	0.507	0.431	0.378
15	0.996	0.723	0.540	0.426	0.349	0.298
20	0.997	0.676	0.492	0.385	0.314	0.267
Γ = 1.91	μ					
$\overline{U}$ (ms^{-1})	1	2	3	4	5	6
0.5	0.998	0.989	0.973	0.948	0.936	0.930
5	0.994	0.828	0.680	0.581	0.511	0.462
10	0.994	0.706	0.523	0.420	0.347	0.299
15	0.996	0.683	0.491	0.388	0.316	0.270
20	0.995	0.652	0.466	0.368	0.301	0.257

Since SRFs presented here represent mean values, a measure of dispersion is required. This is provided in terms of their coefficient of variation (COV) defined as the ratio between the standard deviation and associated mean. This is shown in Fig. 15 whilst COV values represented in Fig. 15c are provided in Table 9.

.**FIGURE 15**

Table 9. COV R'_μ averaged across all buildings and periods of vibration.

μ	$\overline{U}$ (ms^{-1})				
	0.5	5	10	15	20
1	0.0173	0.0056	0.0231	0.0035	0.0050
2	0.1831	0.1847	0.1603	0.1680	0.1261
3	0.2436	0.2604	0.2241	0.2307	0.1758
4	0.2720	0.3164	0.2626	0.2696	0.1972
5	0.3141	0.3577	0.2940	0.2956	0.2133
6	0.3557	0.3922	0.3089	0.3123	0.2232

It is seen in Fig. 15 and Table 9 that COV changes with T, μ, $\overline{U}$, and across all Buildings. Lower dispersion is seen for the lower and higher periods of vibration whereas COV increases with μ which is apparently due to the increase of response amplitudes. In general, the fluctuations found around values of R'_μ are comparable with previous studies – see for example Miranda and Ruiz-Garcia (2002), Vidic et al. (1994), and Nassar and Krawinkler (1991).

6.1 Impact of epicentral distance (ED)

Table 1 contains earthquake records with ED ranging between 0.56-57.13 km. This database is consistent with those used to develop the reference models listed in Table 2. However, according to Gillie et al. (2010), Bray and Rodriguez-Marek (2004), and Chopra and Chintanapakdee (2001), amongst others, NF ground motions, which are those located within ~20km from the source, may induce higher strength demands to buildings than FF motions and hence the results presented above for near to zero wind conditions could be non-conservative for certain regions. Thus, in order to assess the impact of ED on those results, SRFs were calculated for two sets each formed by 10 NF and 10 FF earthquake records taken from Table 1. The former corresponds to the series #9, #10, #23 to #30 (ED $\leq$ 7.05 km) whereas the latter includes series #11 to #20 (ED > 22 km). This analysis has shown that for zero wind conditions SRFs for NF ground motions, here termed $R'_{\mu, NF}$ are lower than those located in the FF regions ($R'_{\mu, NF}$) for most period of vibrations and ductility factors – see Fig. 16a.

FIGURE 16

Fig. 16a shows that the value of R'_μ calculated by taking into account all ground motions listed in Table 1 could be over- or under-estimated for any ductility level. The differences found for the ratio $R'_{\mu, NF}$ / $R'_{\mu, FF}$ are within the range 0.9-1.1 with the following mean values calculated across all periods of vibration: 1.002 (μ=1), 1.0 (μ=2), 0.976 (μ=3), 0.955 (μ=4), 0.952 (μ=5), and 0.94 (μ=6). Hence, an underestimation of ~6% could occur if one applies $R'_{\mu, FF}$ to calculate design forces for NF structures. However this condition seems only applicable to near-zero wind conditions as the study reveals that, by increasing the wind speed the ratio $R'_{\mu, NF}$ / $R'_{\mu, FF}$ moves towards the threshold value of 1 up. Fig. 16b shows values of $R'_{\mu, NF}$ / $R'_{\mu, FF}$ averaged across all wind speeds (excluding the zero-wind condition) for each ductility level whereas Fig. 16c shows values of $R'_{\mu, NF}$ / $R'_{\mu, FF}$ averaged across all ductility levels for each wind speed. These results suggest that SRFs calculated with a mix of NF and FF ground motions could under- or over-estimate strength demands for NF conditions. The ratio $R'_{\mu, NF}$ / $R'_{\mu, FF}$ shown in Fig. 16c has the following mean values and COV calculated across all ductility levels: 0.971/0.033 ($\overline{U}$ = 0.0 ms^{-1}), 0.974/0.030 ($\overline{U}$ = 0.5 ms^{-1}), 1.016/0.038 ($\overline{U}$ = 5 ms^{-1}), 1.049/0.036 ($\overline{U}$ = 10 ms^{-1}), 1.079/0.033 ($\overline{U}$ = 15 ms^{-1}), and 1.041/0.021 ($\overline{U}$ =20

ms^{-1}). Hence, based on these results one could expect differences within ± 8% with dispersion levels of up to 4% between the results presented above and those calculated for NF or FF conditions, being the results reported here on the conservative side for any wind level above $\overline{U}$ = 0.5 ms^{-1}.

7. Joint probabilities of earthquake and wind events: an insight

The probability of occurrence of wind velocity can be established through the Weibull distribution function whose general form is given in Eq. 7. The constants *k* and *c* are the shape and scale parameter respectively, which vary from place to place. These are linked to local conditions including latitude, orography, soil roughness and seasonal effects.

$$P(\overline{U}) = \frac{k}{c}\left(\frac{\overline{U}}{c}\right)^{k-1} e^{-\left(\overline{U}/c\right)^{k}} \quad (7)$$

The determination of the average wind velocity in a place thus requires knowledge of a number of factors. However, it is possible to establish an interval for *k* and *c* based on full-scale measurements – see for example van Donk et al. (2005), Waewsak et al. (2011), and Azad et al. (2014). We could thus take those intervals to be 2.5 ≤ *k* ≤ 4.5 and 2 ≤ *c* ≤ 8 to characterise monthly averages. This yields probability distribution functions such as those shown in Fig. 17.

FIGURE 17

By integrating Eq. (12) whilst using the intervals for *k* and *c* established above the value of $\overline{U}$ that is exceeded 25%, 50%, and 75% of the time has been inferred. This is shown in Table 10.

Table 10. Values of $\overline{U}$ which are exceeded 25%, 50%, and 75% of time given *k* and *c*.

k	% time $\overline{U}$ is exceeded	*c*						
		2	3	4	5	6	7	8
2	25	1.63	2.45	3.26	4.04	4.75	5.33	5.77
	50	0.96	1.44	1.91	2.38	2.81	3.18	3.49
	75	0.46	0.68	0.91	1.13	1.33	1.51	1.67
2.5	25	1.85	2.77	3.69	4.60	5.47	6.19	6.74
	50	1.27	1.90	2.53	3.15	3.76	4.29	4.72
	75	0.76	1.13	1.51	1.88	2.25	2.57	2.84
3	25	1.94	2.91	3.88	4.85	5.80	6.64	7.27
	50	1.45	2.17	2.89	3.62	4.33	4.98	5.51
	75	0.98	1.46	1.95	2.43	2.91	3.36	3.74
3.5	25	1.99	2.99	3.98	4.98	5.97	6.89	7.60
	50	1.57	2.35	3.13	3.91	4.69	5.43	6.04
	75	1.14	1.70	2.27	2.83	3.40	3.94	4.40
4	25	2.02	3.03	4.04	5.05	6.05	7.03	7.81
	50	1.65	2.47	3.29	4.11	4.93	5.73	6.42
	75	1.26	1.88	2.51	3.13	3.76	4.37	4.91
4.5	25	2.04	3.05	4.07	5.09	6.10	7.10	7.95
	50	1.70	2.55	3.40	4.25	5.10	5.94	6.70
	75	1.35	2.02	2.69	3.36	4.04	4.70	5.31

Furthermore, the frequency of occurrence of earthquakes given their magnitude can be estimated by using the Gutenberg-Richter law quoted in Eq. (8).

$$log_{10}N = a - bM \quad (8)$$

where N is the number of earthquakes of magnitude $\geq M$ and a, b are constants.

Following, a reference seismic magnitude associated to a 50-year return period (T_{50}) can be established by using a = 8.44 and b = 1.06 in Eq. (13), as in Sharma et al. (1999) where a global magnitude-frequency analysis of data was undertaken. Table 11 shows this and 9 other values of seismic magnitude and associated probabilities.

Table 11. Probabilities associated to earthquake and wind events

Row / Column		1	2	3	4	5	6	7	8	9	10
1	M_s	9.565	9.4	9.3	9.2	9.1	9.0	8.9	8.8	8.7	8.6
2	T_{EQ} ~	50	33	26	21	16	13	10	8	6	5
3	P_{EQ}	0.02	0.029	0.038	0.049	0.062	0.079	0.101	0.129	0.165	0.211
4	P_{wind}	1.00	0.668	0.524	0.410	0.321	0.252	0.197	0.155	0.121	0.095
5	$\overline{U}$ ms^{-1}	0.00	4.35	5.34	6.11	6.74	7.25	7.70	8.07	8.4	8.67

The reference magnitude for T_{50} is 9.565. Table 11 provides ten cases in which the joint probabilities of occurrence of earthquake and wind events equal that of P_{50} = 0.02. These values were estimated by considering Weibull parameters k = 3 and c = 8 which are within the range shown in Table 10. Row 4 in Table 11 thus indicates the probability that the k-th wind velocity ($\overline{U}$) is exceeded (according to Eq. (7)) whereas the product of rows 3 and 4 gives a joint probability of 0.02. This simple analysis evidences the potential impact of the combined events. For example, given an earthquake whose return period is of 5 years – see col. 10 in Table 11, a value of $\overline{U} = 8.67$ ms^{-1} would need to occur to match the condition P_{joint} = 0.02. Moreover, in row 5 it is shown that strong earthquakes whose magnitude oscillates between 9.4 and 8.6 would induce the reference probabilities of occurrence (P_{50} = 0.02) shall they occur simultaneously with wind events whose average velocity oscillates between 4.35 ms^{-1} and 8.67 ms^{-1}. Evidently as the earthquake magnitude decreases lower energy levels would be imparted to structures exposed to such events. However as per the results shown in Table 5, the ratio F^*_{EQ}/F^*_W decreases at high rates with the increase of $\overline{U}$. That ratio is on average (across all buildings) of 2.45, 0.62, and 0.27 for $\overline{U} = 5$ ms^{-1}, 10 ms^{-1}, and 15 ms^{-1}, respectively. This means that as one moves right in Table 11 wind forces would increase at higher rates than the decrease of earthquake forces. A critical condition can be identified in Table 5 where for the x-direction of Building 3 there is a ratio $F^*_{EQ}/F^*_W = 0.79$ when $\overline{U} = 5$ ms^{-1}. Finally, in section 6 above is shown that when $\overline{U} = 5$ ms^{-1} the ratio R'_μ / R_μ would oscillate between 0.958 and 0.565, depending on the value of Γ and for $2 \leq \mu \leq 6$. From the data shown in Table 11, the joint probability of such wind conditions and earthquakes whose magnitude oscillates between 9.3 and 9.4 matches the reference probabilities of occurrence P_{50} = 0.02. Therefore, the underestimation of design forces under multi-hazard conditions is likely to occur.

8. Conclusions

This investigation shows the impact of considering wind load in the estimation of SRFs. It is shown that the amplitude and shape of the curves $R_\mu - T$ change depending on the wind speed and the ratio between the mass and volume of structures (Γ). This variation is established in terms of the ratio R'_μ / R_μ – where

R_μ and R'_μ represent SRFs calculated by using earthquake load only and combinations of earthquake and wind load, respectively. It is shown that the decrease of R'_μ / R_μ can be between 20% and 60% even for low levels of wind and can go below those limits when $\overline{U}$ increases. The influence of the parameter Γ was also examined and it is concluded that the ratio between earthquake and wind forces decreases with Γ. This reflects the fact that wind gusts acting on a surface correlate better as the area decreases. The paper also highlights that ED can have an impact on SRFs within a range of variation of $\pm$ 8% depending on whether structures are located near of far from faults. On the other hand, a quick analysis of the probabilities of occurrence of wind in normal conditions suggests that wind velocities of 5 ms^{-1} are susceptible of being frequently exceeded whereas those with the range of 5 <. $\overline{U}$ < 10 can also be exceeded 25% of time. The joint probabilities associated to earthquake and wind indicates that SRFs estimated by ignoring the influence of wind are non-conservative. Although it should be noted that the return period of ground motions used for actual design is not be fixed. For example the USA Building Seismic Safety Council provides inelastic spectra associated to return periods ranging between 25 and 505 years (Malhotra, 2005) - San Francisco and Los Angeles California have inelastic spectral ordinates corresponding to 30-50 years and 25-30 years respectively whilst Charleston South Carolina uses inelastic spectral ordinates whose return period ranges between 375 and 505 years. Hence in such a framework the influence of wind on earthquake design forces would have different levels of impact depending on the criteria for regionalisation. Finally, it seems advisable to take into consideration wind and earthquake combined effects by decreasing strength reduction factors rather than by modifying load combination factors for wind in combinations in which seismic actions are the main variable action. That is because the ratio between earthquake and wind load is highly susceptible to level of wind load. Hence for different levels of wind speeds, different strength reduction factors would apply.

References

Amos J, 2015. Unsettled earth continues to rattle Nepal. BBC News -12 May 2015.

ANSI/ASCE 7-95, 1996. American Society of Civil Engineers.

Azad A K, Rasul M G, Yusaf T, 2014. Statistical diagnosis of the best Weibull methods for wind power assessment for agricultural applications. Energies. 7: 3056-3085.

Bray J D, Rodriguez-Marek A, 2004. Characterization of forward-directivity ground motions in the near-fault region. Soil Dynamics and Earthquake Engineering, 24: 815-828.

Chopra A K, 1995. Dynamics of structures: theory and applications to earthquake engineering, Prentice Hall.

Chopra A K, Goel R K, 1999. Capacity-demand-diagram methods based on inelastic design spectrum. Earthquake Spectra, **15**(4): 637-656.

Chopra A K, Chintanapakdee C, 2001. Comparing response of sdf systems to near-fault and far-fault earthquake motions in the context of spectral regions. Earthquake Engineering and Structural Dynamics, 30: 1769-1798.

Daniell J E, Khazai B, Wenzel F, 2011. The CATDAT damaging earthquake database. Natural Hazards and Earthquake Sciences, **11**: 2235-2251.

Davenport A G, 1967. Gust loading factors. American Society of Civil Engineering Paper **5255**: 11-34.

Dyrbye C, Hansen S, 1997. Wind loads on structures. John Wiley and Sons.

EC8, 2011. Design of structures for earthquake resistance. European Committee for Standardization.

Elghadamsi F E, Mohraz B, 1987. Inelastic earthquake spectra. Earthquake Engineerng and Structural Dynamics, **15**: 91-104.

ESDU 85020, 2001. Characteristics of atmospheric turbulence near the ground. Engineering Sciences Data Unit.

FEMA P695, 2009. Quantification of building seismic performance factors. Applied Technology Council.

Gillie J L, Rodriguez-Marek A, McDaniel C, 2010. Strength reduction factors for near-fault forward directivity ground motions. Engineering Structures, 32: 273-285.

Hidalgo P, Arias A, 1990. New Chilean code for earthquake-resistant design of buildings. Proc. Fourth U S National Conference on Earthquake Engineering, 2: 927-936.

Lai S P, Biggs J M, 1980. Inelastic response spectra for aseismic building design. J Struct. Div. ASCE, 106(6): 295-1310.

Malhotra P, 2005. Return period of design ground motions. Seismological Research Letters, 76(6): 693-699.

Martinez-Vazquez P, Rodriguez-Cuevas N, 2007. Wind field reproduction using neural networks and conditional simulation. Engineering Structures. 29: 1442-1449.

Miranda E, 1993. Site-dependent strength reduction factors. J Struct. Eng. ASCE, 119(5): 1319-1338.

Miranda E, Bertero V, 1994. Evaluation of strength reduction factors for earthquake-resistant design. Earthquake Spectra, 10(2): 357-379.

National Building Code of Canada, 2015. Canadian Commission of Building and Fire Codes.

Nassar A, Krawinkler H, 1991. Seismic demands for SDOF and MDOF systems. The John A Blume Earthquake Eng. Centre Stanford University, 95.

Newmark N M, Hall W J, 1973.Seismic design criteria for nuclear reactor facilities. Building Practices for Disaster Mitigation, National Bureau of Standards, 46: 209-236.

Newmark N M, Hall W J, 1982. Earthquake spectra and design. Earthquake Eng. Research Institute.

Pacific Earthquake Engineering Research Centre (PEER). PEER ground motion database http://ngawest2.berkeley.edu/#disclaimer [accessed on 19.03.2016].

Simiu E, Scanlan H, 1978. Wind effects on structures: an introduction to wind engineering. Wiley.

Sharma R D, Gupta S, Kumar S, 1999. Application of extreme-value distribution for estimating earthquake magnitude-frequency relationships. J. Earthquake Technology, 388(36): 15-26.

Riddell R, Newmark N M, 1979. Statistical analysis of the response of non-linear systems, 468.

Riddell R, Hidalgo P, Cruz E, 1989. Response modification factors for earthquake resistant design of short period structures. Earthquake Spectra, 5(3): 571-590.

Riddell R, Garcia J E, Garces E, 2002. Inelastic deformation response of SDOF systems subject to earthquakes. Earthquake Eng. Struct. Dyn. 31: 515-538.

Tanaka H, Lawen N, 1986. Test on the CAARC standard tall building model with a length scale of 1:1000. J. Wind Eng. Ind. Aerodyn. 25: 15-29.

Van Donk S J, Wagner L E, Skidmore L, Tatarko J, 2005. Comparison of the Weibull model with measured wind speed distributions for stochastic wind generation. American Soc. Agricultural Eng. 48(2): 503-510.

Vanmarcke E, Heredia-Zavoni E, Fenton G, 1993. Conditional simulation of spatially correlated ground motion. J. Eng. Mech. 119(11): 2333-2352.

Vidic T, Fajfar P, Fischinger M, 1992. A procedure for determining consistent inelastic design spectra. Proc. Workshop on Nonlinear Seismic Analysis of RC Structures. Bled, Slovenia, July.

Vickery B J, 1970. On the reliability of gust loading factors. Proc. Technical Meeting Concerning Wind Loads on Buildings and Structures. Build. Sc. Ser. 30. Ntl. Bureau of Standards, Washington DC 93-104.

Waewsak J, Chancham C, Landry M, Gagnon Y, 2011. An analysis of wind speed distribution at Thasala, Nahkohn Si Thammaray, Thailand. J. Sustainable Energy & Environment. 2: 51-55.

Appendix

Wind forces acting on point-like structures can be calculated through Eq. (A1) – where ρ represents the density of air, C_D is a drag coefficient, $U_T(t)$ is the total wind speed at the time t, and A is the area exposed. The total wind speed can in turn be expressed in terms of the mean and dynamic components, $\overline{U}$ and $u(t)$ as in Eq. (A2).

$$F_w(t) = \frac{1}{2}\rho C_D U_T(t)^2 A \quad \text{(A1)}$$

$$F_w(t) = \frac{1}{2}\rho C_D [\overline{U} + u(t)]^2 A \quad \text{(A2)}$$

$$u(t) = \sigma_z \left(\frac{1}{N}\right)^{1/2} \sum_{k=1}^{N} \cos(2\pi n_k t + \phi_k) \quad \text{(A3)}$$

$$g(n_k) = \frac{S(n_k)}{\sigma_z^2};\ h(\varphi_k) = \frac{1}{2\pi} \quad \text{(A4)}$$

$$\frac{nS(n_k)}{\sigma^2} = \frac{4\left(\frac{nL}{\overline{U}}\right)}{\left(1+70.8\left(\frac{nL}{\overline{U}}\right)^2\right)^{5/6}} \quad \text{(A5)}$$

The required zero-mean wind time series of $u(t)$ can be found with Eq. (A3) as in Simiu and Scanlan (1978). In this equation σ_z denotes variance of wind velocity at the reference height z; n_k and φ_k are respectively the *k-th* gust frequency and random number that identifies a phase angle valid within the range $0 \leq \varphi_k < 2\pi$. The vectors containing all values of n_k and φ_k are characterised by having probability distributions $g(n_k)$ and $h(\varphi_k)$ of the form shown in Eq. (A4). This equation requires the wind power spectrum ($S(n_k)$) to be known. To tha end the Von Karman model quoted in Eq. (A5) can be used together with a length scale (L) of 150 m (ESDU 85020, 2001).

In this research wind time series were generated for a terrain located in the countryside whilst the turbulence intensity defined as $I = \sigma/\overline{U}$ was taken as 0.295 and assumed to be constant at the lower part of the atmospheric boundary layer.

Figure Captions

Fig. 1 Relationship between restoring force (F) and structural deformation (u).

Fig. 2 Estimated strength reduction factors (a) and their comparison with the model proposed by (b) Ridell, Hidalgo, and Cruz, 1989.

Fig. 3 Estimated strength reduction factors and their comparison with the models proposed by (a) Hidalgo and Arias, 1990, and (b) Nassar and Krawinkler, 1991.

Fig. 4 Estimated strength reduction factors and their comparison with the models proposed by (a) Vidic, Fajafar and Fischinger, 1992, and (b) Miranda and Bertero (1994).

Fig. 5 Comparison of normalised strength reduction factors.

Fig. 6 Geometry of full-scale structures for analysis.

Fig. 7 Strength reduction factors estimated for when $\bar{U}$ = 0.5 ms^{-1} and (a) Γ=60.43, (b) Γ=17.78, and (c) Γ=1.91.

Fig. 8 Strength reduction factors estimated for when $\bar{U}$ = 5 ms^{-1} and (a) Γ=60.43, (b) Γ=17.78, and (c) Γ=1.91.

Fig. 9 Strength reduction factors estimated for when $\bar{U}$ = 10 ms^{-1} and (a) Γ=60.43, (b) Γ=17.78, and (c) Γ=1.91.

Fig. 10 Strength reduction factors estimated for when $\bar{U}$ = 15 ms^{-1} and (a) Γ=60.43, (b) Γ=17.78, and (c) Γ=1.91.

Fig. 11 Strength reduction factors estimated for when $\bar{U}$ = 20 ms^{-1} and (a) Γ=60.43, (b) Γ=17.78, and (c) Γ=1.91.

Fig. 12 Variation of R'_{μ} / R_{μ} with μ and T for when Γ = 1.91 and (a) $\bar{U}$ = 0.5 ms^{-1}, and (b) $\bar{U}$ = 5 ms^{-1}.

Fig. 13 Variation of R'_{μ} / R_{μ} with μ and T for when Γ = 1.91 and (a) $\bar{U}$ = 10 ms^{-1}, and (d) $\bar{U}$ = 20 ms^{-1}.

Fig. 14 Variation of R'_{μ} / R_{μ} with Γ, averaged across all ductility levels when (a) $\bar{U}$ = 5 ms^{-1}, (b) $\bar{U}$ = 10 ms^{-1}, and (c) $\bar{U}$ = 20 ms^{-1}.

Fig. 15 COV related to the estimated values of R'_{μ}: (a) for all periods of vibrations and buildings, when μ = 3 and $\bar{U} = 10$ ms^{-1} ($COV_{\mu=3}$); (b) for all periods of vibration and ductility levels, averaged across all buildings and velocity levels ($COV_{B,U}$); and (c) for all ductility and velocity levels, averaged across all buildings and periods of vibration ($COV_{B,T}$).

Fig. 16 Relationship $R'_{\mu,NF} / R'_{\mu,FF}$ calculated for (a) zero-wind conditions; (b) averaged across all wind speeds: in the range 0.5 ms^{-1} to 20 ms^{-1} and (c) averaged across all ductility levels.

Fig. 17 Weibull distribution for wind velocities in normal conditions.

11 March, 2017

Dear Sir/Madame,

Many thanks again for the update on the paper and for letting me have the latest comments of the reviewers. The changes made did not significantly increased the number of words with respect to that established in the previous submissions – passing from 6180 to 6221. However, after addressing the final comment by the reviewers, regarding the need to split figures which occupied more than one row of images, the number of figures passed from 10 to 17. Noting that now new figures have been produced, the increase was purely due to the way in which figures have been re-numbered.

I enclose a table showing how the reviewers' comments have been addressed together with the electronic files that constitute the reviewed manuscript.

May I thank you again for your kind attention and hope to hear from you soon,

Regards,

Dr Pedro Martinez-Vazquez

Lecturer in Civil Engineering || University of Birmingham || United Kingdom|| Tel. +44 121 414 5059

Reviewer #	Comment	Response
2	suggested insertion in first sentence of introduction "for performance-based design" after 'the world'	The change has been made
4	The response of the authors is debatable. For long periods, say T>2s, the response to seismic actions tends to be dominated by higher modes as the 1st mode has little influence on the dynamic behaviour, since the dominating periods of the seismic actions are usually below T=2s. The same does not happens with the wind action, since the frequency contents of this action is shifted to the side of low frequencies (high periods) as compared to the seismic action. So it suggested to the authors to improve their justification, if they wish. This is left for the authors to decide	The author agrees with the reviewer in the sense that earthquake and wind load are associated to different frequency contents and hence higher-order modes could have slightly different impact when estimating earthquake and wind effects. However, it does not seem that such fluctuations would revert the key conclusions reached by using the generalise method i.e. quantitative but not qualitative changes would occur to the main finding of the investigation.
	The response of the authors is clear and satisfactory, but the explanation should also be available to the readers, this is, it should be inserted in the text of the paper	Thanks for making that observation. The paragraph below Table 5 has been amended as follows, *As the area exposed to wind reduces wind gusts increase correlation which results in a lower value of F_{EQ}^{*}/F_{W}^{*} whereas the value of this parameter decreases with $\bar{U}$ as M* keeps constant. Noting that, however the PGA of the seismic actions considered in this study ranges between 0.1g and 0.77g, the variability of the ratio F_{EQ}^{*}/F_{W}^{*} amongst different ranges of PGA e.g. 0.1-0.3PGA, 0.3-0.5PGA, and 0.5-0.7PGA, is within reasonable limits. The results in Table 1 are summarised in Table 6 after averaging the values of F_{EQ}^{*}/F_{W}^{*} considering all earthquake records and wind directions.*
	Figures 1, 3, 4 and 10 are suitable but all the other figures and sub-figures should be each uploaded as separate files. Each figure should start with a, b, c etc not a follow on like Figure 5. Please complete a copyright permission form for your manuscript and if you wish to add author photos you must submit each of them as separate files in jpg.	Figures have been uploaded in separate files. Also, Fig. 2, 5, and 6 (old numbering) have been split in such a way that each row of figures follows the sequence a, b, and c.

Figure 1

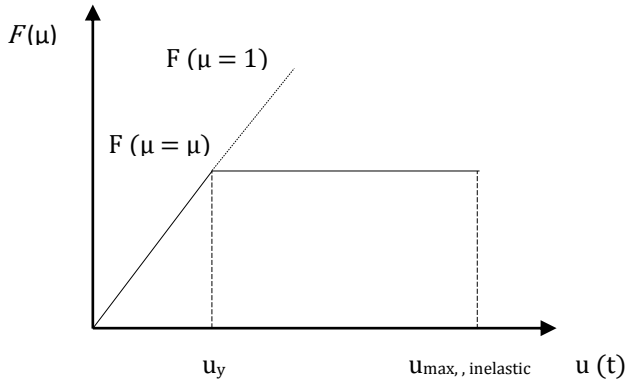

Figure 2a

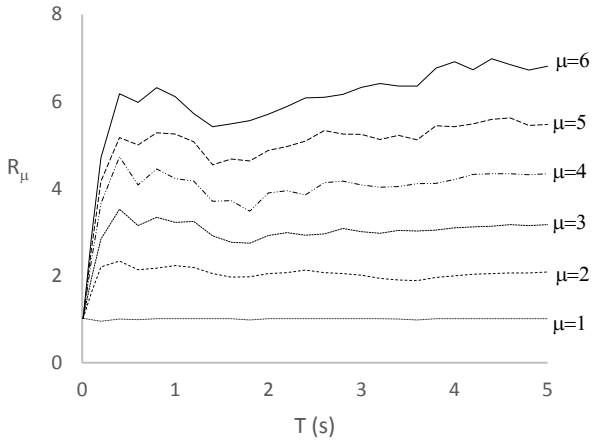

(a)

Figure 2b

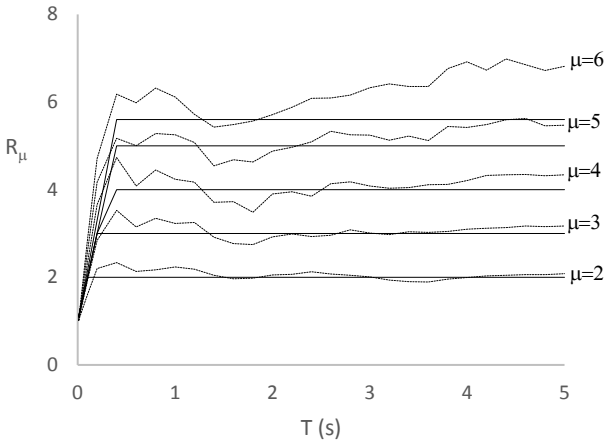

(b)

Figure 3a

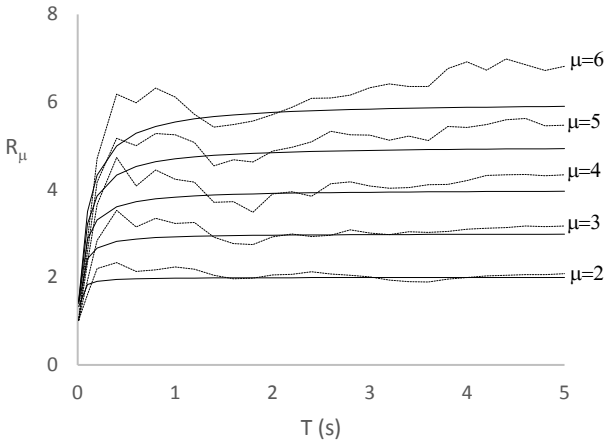

(a)

Figure 3b

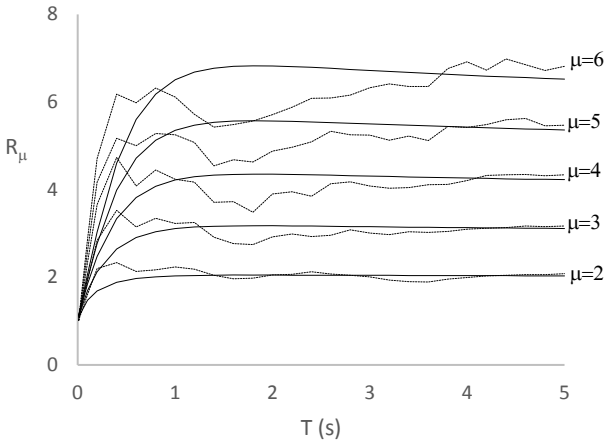

(b)

Figure 4a

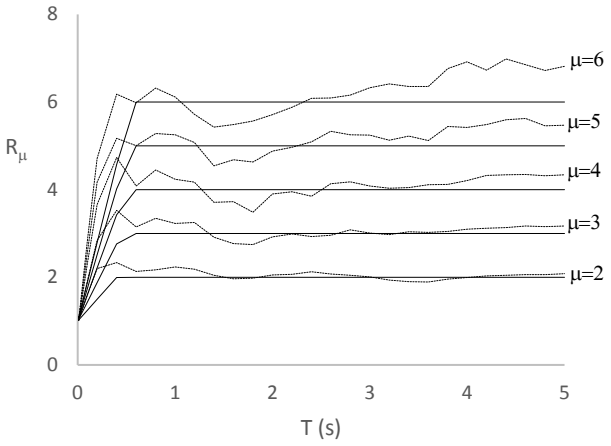

(a)

Figure 4b

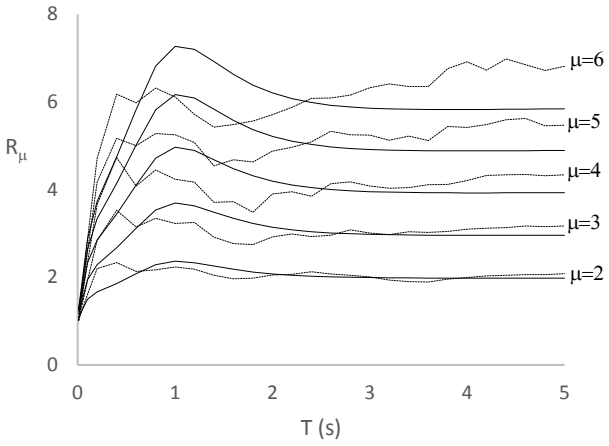

(b)

Figure 5

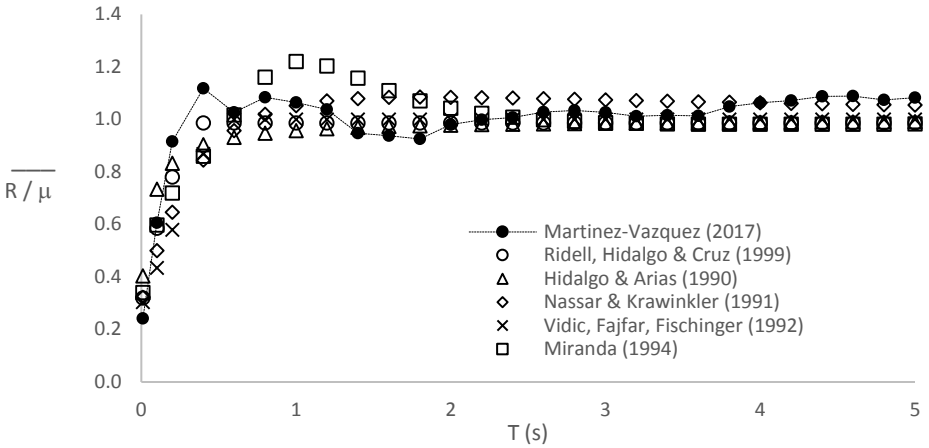
1.4
1.2
1.0
0.8
0.6
0.4
0.2
0.0
R / μ
0
1
2
3
4
5
T (s)
Martinez-Vazquez (2017)
Ridell, Hidalgo & Cruz (1999)
Hidalgo & Arias (1990)
Nassar & Krawinkler (1991)
Vidic, Fajfar, Fischinger (1992)
Miranda (1994)

Figure 6

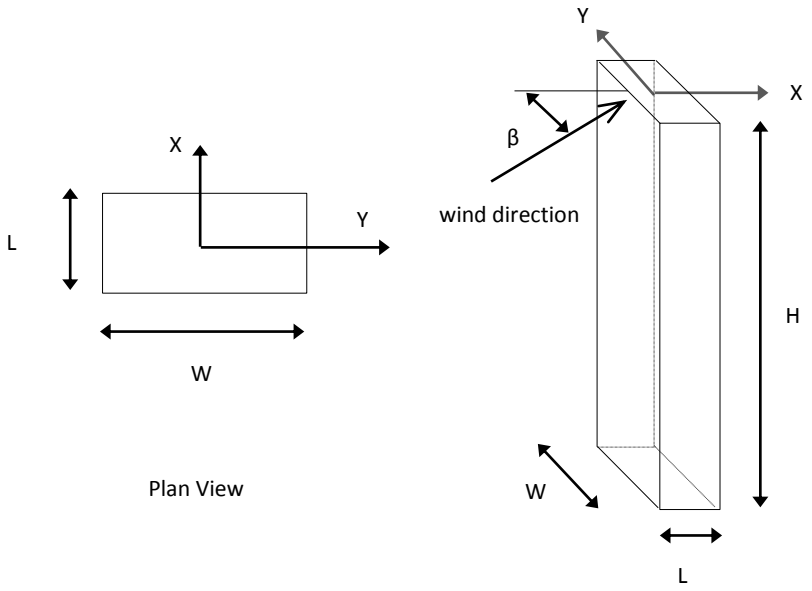

Figure 7a

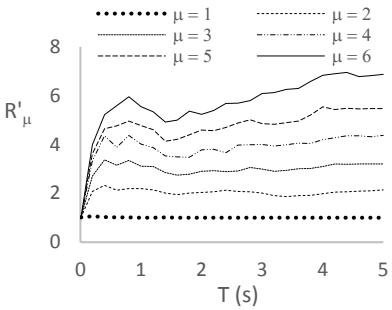

(a) $\Gamma = 60.43, \overline{U} = 0.5\ \mathrm{ms}^{-1}$

Figure 7b

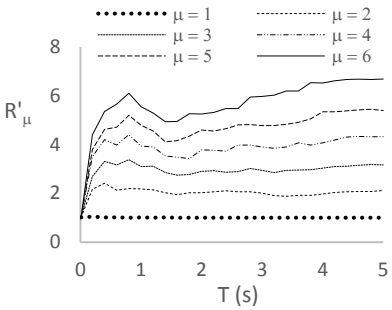

(b) $\Gamma = 17.78, \overline{U} = 0.5\ \mathrm{ms}^{-1}$

Figure 7c

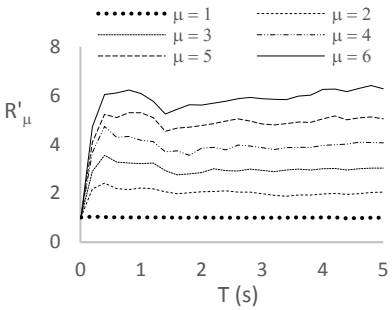

(c) $\Gamma = 1.91, \overline{U} = 0.5\ \mathrm{ms}^{-1}$

Figure 8a

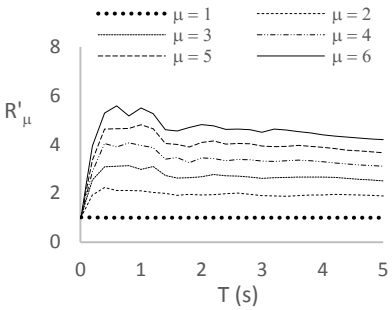

(a) $\Gamma = 60.43, \overline{U} = 5\ \mathrm{ms}^{-1}$

Figure 8b

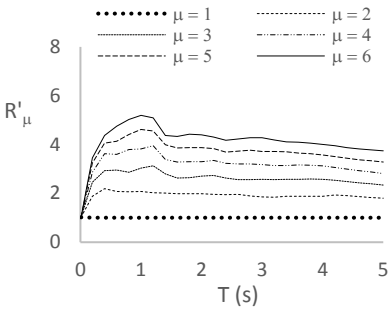

(b) $\Gamma = 17.78, \bar{U} = 5\ \mathrm{ms}^{-1}$

Figure 8c

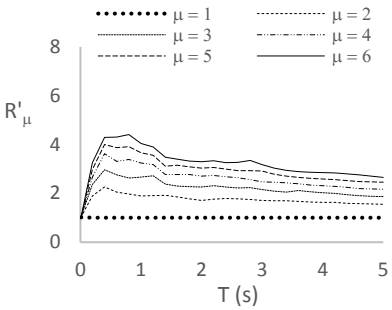

(c) $\Gamma = 1.91, \overline{U} = 5\ \mathrm{ms}^{-1}$

Figure 9a

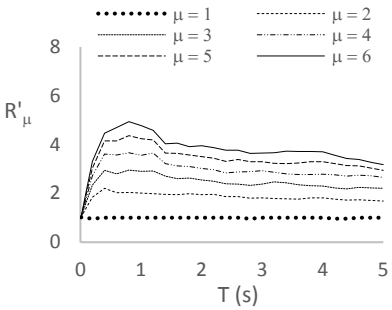

(a) $\Gamma = 60.43, \overline{U} = 10\ \mathrm{ms}^{-1}$

Figure 9b

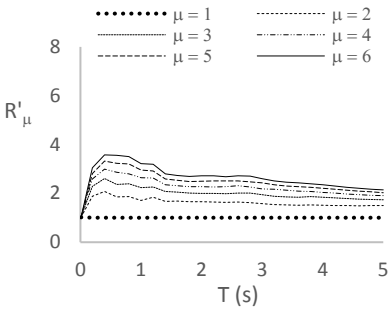

(b) $\Gamma = 17.78, \overline{U} = 10\ \mathrm{ms}^{-1}$

Figure 9c

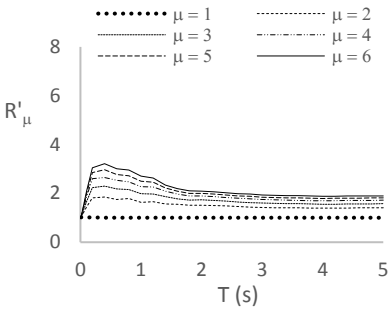

(c) $\Gamma = 1.91, \overline{U} = 10\ \mathrm{ms}^{-1}$

Figure 10a

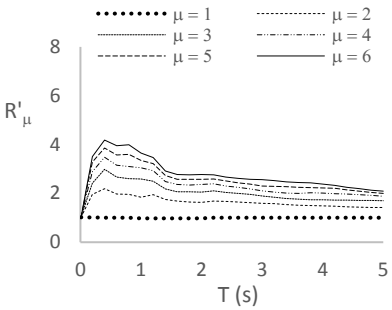

(a) $\Gamma = 60.43, \overline{U} = 15\ \mathrm{ms}^{-1}$

Figure 10b

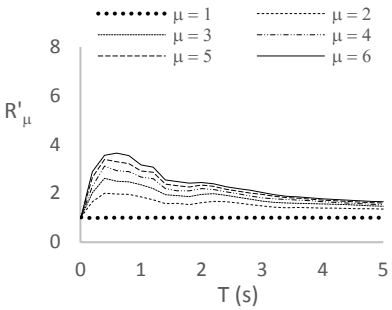

(b) $\Gamma = 17.78, \overline{U} = 15\ \mathrm{ms}^{-1}$

Figure 10c

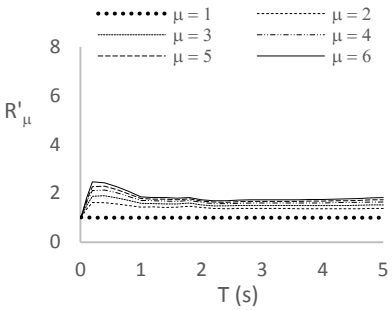

(c) $\Gamma = 1.91, \overline{U} = 15\ \mathrm{ms}^{-1}$

Figure 11a

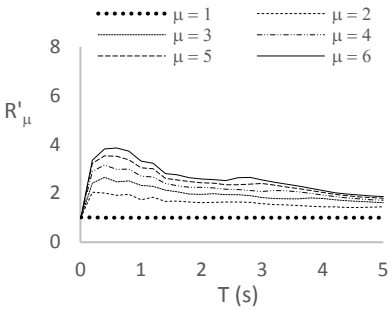

(a) $\Gamma = 60.43, \overline{U} = 20\ \mathrm{ms}^{-1}$

Figure 11b

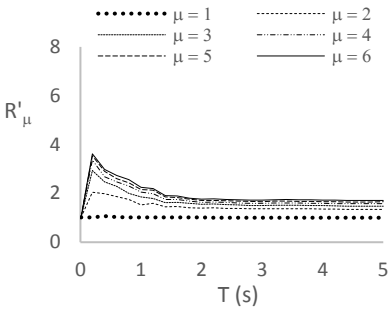

(b) $\Gamma = 17.78, \overline{U} = 20\ \mathrm{ms}^{-1}$

Figure 11c

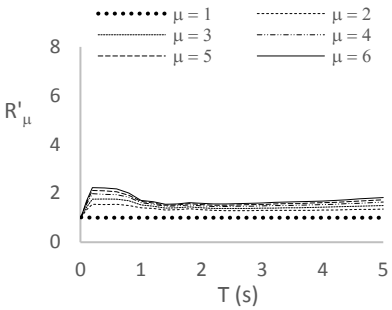

(c) $\Gamma = 1.91, \overline{U} = 20\ \mathrm{ms}^{-1}$

Figure 12a

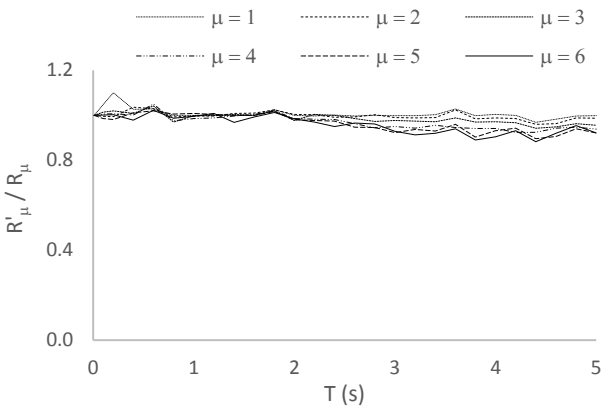

(a)

Figure 12b

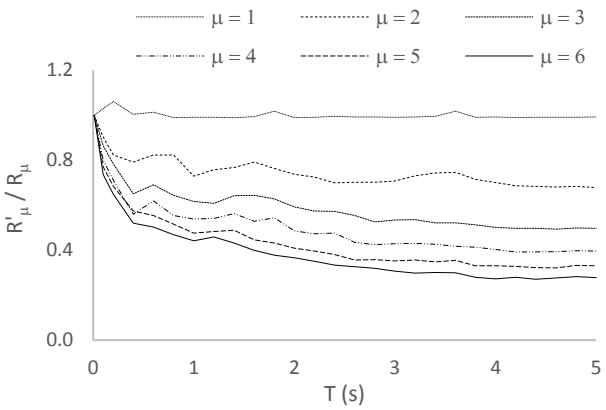

(b)

Figure 13a

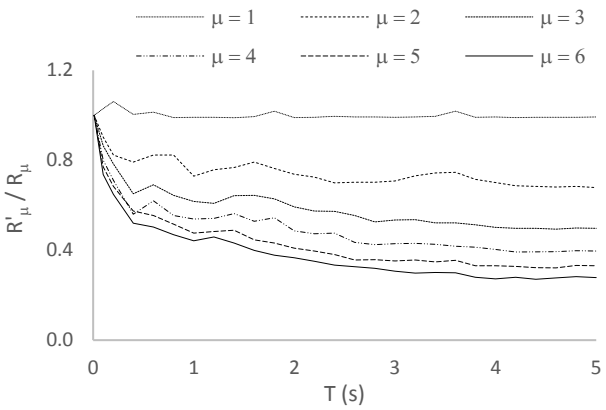

(a)

Figure 13b

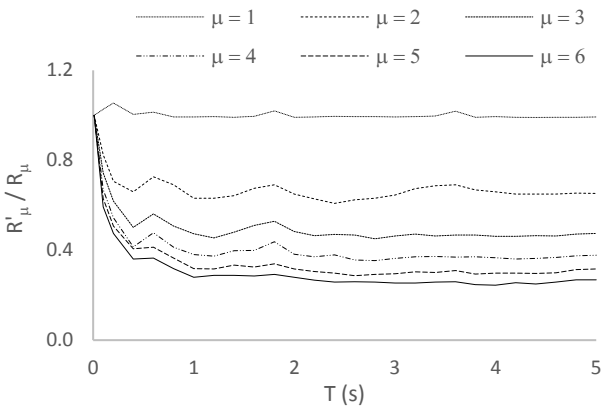

(b)

Figure 14a

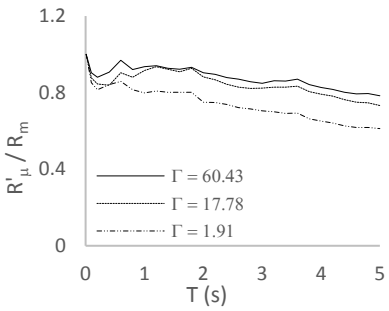

(a)

Figure 14b

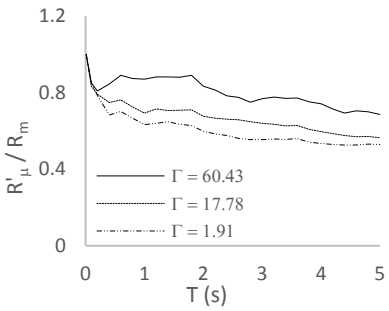

(b)

Figure 14c

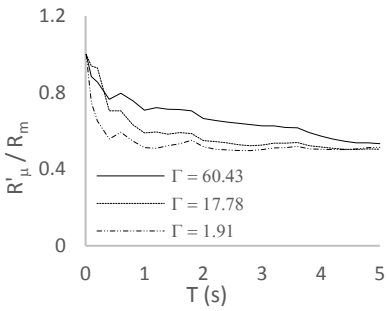

(c)

Figure 15a

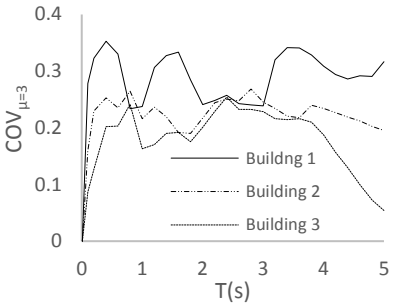

(a)

Figure 15b

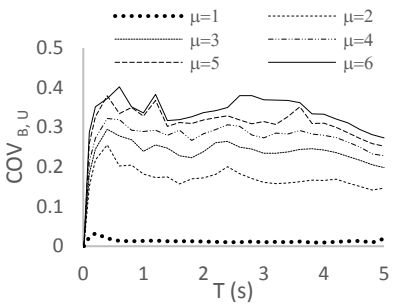

(b)

Figure 15c

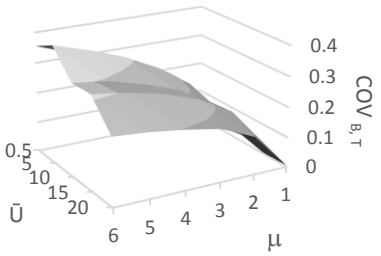

(c)

Figure 16a

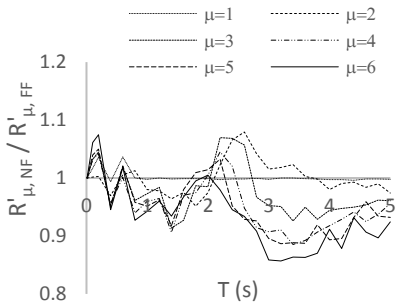

(a)

Figure 16b

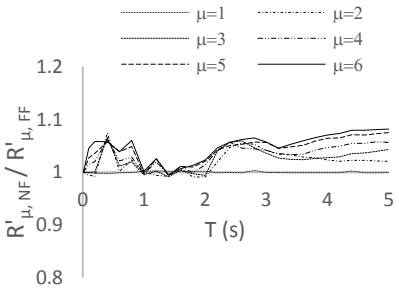

(b)

Figure 16c

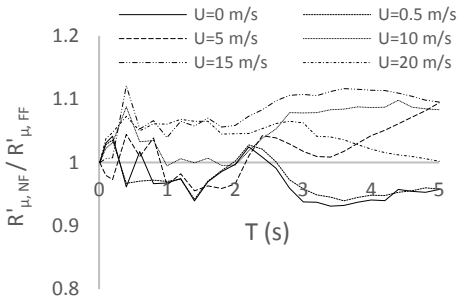
U=0 m/s
U=0.5 m/s
U=5 m/s
U=10 m/s
U=15 m/s
U=20 m/s
1.2
1.1
1
0.9
0.8
0
1
2
3
4
5
T (s)
R'μ, NF / R'μ, FF

(c)

Figure 17

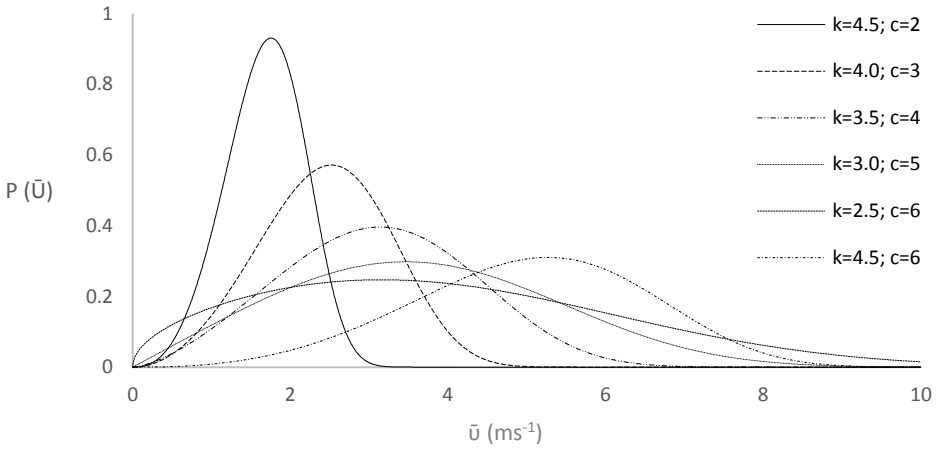
1
0.8
0.6
0.4
0.2
0
P (Ū)
0
2
4
6
8
10
ū (ms-1)
k=4.5; c=2
k=4.0; c=3
k=3.5; c=4
k=3.0; c=5
k=2.5; c=6
k=4.5; c=6